

A source-sink model of the generation of plate tectonics from non-Newtonian mantle flow

David Bercovici

Department of Geology and Geophysics, School of Ocean and Earth Science and Technology
University of Hawaii, Honolulu

Abstract. A model of mantle convection which generates plate tectonics requires strain rate- or stress-dependent rheology in order to produce strong platelike flows with weak margins as well as strike-slip deformation and plate spin (i.e., toroidal motion). Here, we employ a simple model of source-sink driven surface flow to determine the form of such a rheology that is appropriate for Earth's present-day plate motions. In this model, lithospheric motion is treated as shallow layer flow driven by sources and sinks which correspond to spreading centers and subduction zones, respectively. The source-sink field is derived from the horizontal divergence of plate velocities and thus directly prescribes poloidal motion. The toroidal flow field is solved through the non-Newtonian Stokes equation for shallow layer tangential flow on the surface of a sphere. Two plate motion models are used to derive the source-sink field. The first is an idealized "square" plate which is used to explore the basic aspects of the model. The second is an analytically continuous model of Earth's present-day plates (Bercovici and Wessel, 1994). As originally implied in the simpler Cartesian version of this model (Bercovici, 1993), the classical power law rheologies do not generate platelike flows as well as the hypothetical Whitehead-Gans stick-slip rheology (which incorporates a simple self-lubrication mechanism). For the idealized plate geometry, the power law rheologies yield much more diffuse strike-slip shear (i.e., radial vorticity) than the stick-slip rheology. For the present-day plate geometry, the power law rheologies fail to reproduce the original proportion of left- and right-lateral strike-slip shear, whereas the stick-slip rheology gives almost exactly the right proportion. None of the fluid rheologies examined, however, produce more than approximately 60% of the original maximum shear. For either plate model, the viscosity fields produced by the power law rheologies are diffuse, and the viscosity lows over strike-slip shear zones or pseudo-margins are not as small as over the prescribed convergent-divergent margins. In contrast, the stick-slip rheology generates very platelike viscosity fields, with sharp gradients at the plate boundaries, and margins with almost uniformly low viscosity. Quantitative comparisons with the toroidal-poloidal kinetic energy partitioning and vorticity fields of the original plate model are also examined, and the stick-slip rheology is generally found to yield the most favorable comparisons. Power law rheologies with high viscosity contrasts, however, lead to almost equally favorable comparisons, though these also yield the least platelike viscosity fields. This implies that the magnitude of toroidal flow and platelike strength distributions are not necessarily related and thus may present independent constraints on the determination of a self-consistent plate-mantle rheology. The results of this study, however, predict that if such a rheology can indeed be uniquely determined, it is likely to be in the class of stick-slip, self-lubricating rheologies.

Introduction

The physics of thermal convection provides one of the most prevalent underlying principles of atmospheric, astrophysical, oceanographic, and geophysical dynamics.

To each field, convection yields a unique enigma, e.g., the Great Red Spot in the atmospheric circulation of Jupiter, or the generation of magnetic fields in stellar and planetary interiors. For convection in the solid mantle of Earth, perhaps the greatest enigma is plate tectonics itself. Since the plates circulate through the mantle, they are necessarily part of the overall convective flow, and their surface motion represents the horizontal planform of some form of thermal convection. However, the plates are nothing like basic fluid-

Copyright 1995 by the American Geophysical Union.

Paper number 94JB02598.
0148-0227/95/94JB-02598\$05.00

dynamical convective flow. Narrow spreading zones occur where there are no upwelling currents to force them open [Lachenbruch, 1976]. Downwellings are asymmetrical such that only one side of a convergent zone sinks [e.g., Gurnis and Hager, 1988; King and Hager, 1990]. Deformation is almost entirely focused in narrow bands, while the majority of the flow field is composed of nearly rigid blocks [e.g., Weinstein and Olson, 1992]. Finally, there is the generation of an apparently superfluous flow field. A large part of the motion at Earth's surface involves convergence and divergence (called poloidal flow) and is common to all classical forms of convection. It is associated with upwellings and downwellings and provides the mechanism through which gravitational energy (or heat) is released. However, an almost equal amount of motion is generated which is unseen in most forms of thermal convection and seemingly accomplishes little apart from dissipating energy; this motion is called toroidal flow and represents strike-slip shear and plate spin [Hager and O'Connell, 1978, 1979, 1981; Kaula, 1980; Kaula and Williams, 1983; Forte and Peltier, 1987; Gable et al., 1991; O'Connell et al., 1991; Olson and Bercovici, 1991]

These enigmatic features of the plate tectonic form of mantle convection are typically assumed to arise from Earth's complicated deformation mechanisms, i.e., rheology [Kaula, 1980]. Indeed, as the flowing mantle becomes a tectonic plate, it goes from displaying largely fluid behavior to nonfluid behavior such as both continuous (plastic) and discontinuous (brittle) failure. The rifting of the surface at spreading centers is most probably forced by subducting slabs at great distances and this requires nearly rigid stress guides. Moreover, the existence of toroidal motion in the mantle's creeping style of convection is only mathematically assured in fluid which allows lateral variations in viscosity [e.g., Chandrasekhar, 1961; Kaula, 1980; Christensen and Harder, 1991].

To obtain a unified theory of plate tectonics and mantle convection, it is of primary importance to determine a plate-mantle rheology which allows plate tectonics to arise self-consistently from a convecting mantle. Given the very nature of plates (with strong, slowly deforming interiors and weak, rapidly deforming margins), the strength or viscosity of the plate-mantle material must be dependent on the deformation rate and hence the velocity field. Candidate rheologies have either viscosities dependent on temperature (which, through convection, is itself a nonlinear function of velocity) and/or are non-Newtonian wherein viscosity is explicitly stress- or strain rate-dependent.

In this paper, we seek the rheology which interacts with the so-called convective part of the plate velocity field, the divergent or poloidal field, to yield (1) the non-convective or toroidal (strike-slip and spin) field and (2) platelike strength (or viscosity) distributions. Our theoretical model is composed of a shallow fluid layer (the lithosphere) driven by sources and sinks; these are de-

rived from the plates' divergent-convergent motion and thus represent spreading centers and subduction zones, respectively. The rheologies we examine are not limited to classical mantle-silicate rheologies [e.g., Weertman and Weertman, 1975; Ranalli, 1987] since we wish to describe platelike behavior and not just mantle creep; it is also unlikely that the empirically derived silicate rheologies are sufficient to obtain plate behavior [Christensen and Harder, 1991; Weinstein and Olson, 1992; Bercovici, 1993].

This paper is the companion study to an earlier paper which examined this problem with an idealized Cartesian model [Bercovici, 1993]. Here, we present the spherical version of the model and incorporate present-day motions of Earth's tectonic plates.

Theory

The essence of the non-Newtonian source sink model with consideration for model assumptions is discussed by Bercovici [1993]. We summarize the salient points here which are necessary for development of the spherical model.

Kinematics

The theory only allows horizontal motions within a thin spherical fluid (lithospheric) layer. The horizontal velocity field is divided into its poloidal and toroidal components through a Helmholtz relation

$$\underline{v}_H = \nabla_H \Phi + \nabla \times (\Psi \hat{r}) \quad (1)$$

where $\underline{v}_H = (0, v_\theta, v_\phi)$ is the horizontal velocity vector,

$$\nabla_H = \left(0, \frac{1}{r} \frac{\partial}{\partial \theta}, \frac{1}{r \sin \theta} \frac{\partial}{\partial \phi} \right) \quad (2)$$

is the horizontal gradient, Φ is the poloidal scalar potential, and $\Psi \hat{r}$ is the toroidal vector potential (\hat{r} is the unit normal in the radial direction). As always, r , θ , and ϕ are spherical coordinates, i.e., radius, colatitude, and longitude. Horizontal flow is driven by a field of sources and sinks, i.e., a prescribed horizontal divergence field $D = \nabla_H \cdot \underline{v}_H$. The poloidal potential is thus determined by the source-sink field via Poisson's equation

$$\nabla_H^2 \Phi = D. \quad (3)$$

The fluid is assumed incompressible (i.e., $\nabla \cdot \underline{v} = 0$, where \underline{v} is the complete velocity vector), and although vertical velocity v_r is itself assumed negligible in the layer, we still require that its vertical gradient is

$$\frac{\partial v_r}{\partial r} = -D \quad (4)$$

which is used in the second strain rate invariant for the non-Newtonian viscosity. Equation (4) simply states that there is mass ejection and injection through the

bottom boundary of the layer (assuming the top is impermeable), to or from the underlying medium. However, it is important to note that v_r is only truly negligible if the fluid layer is infinitesimally thin.

Dynamics: The Toroidal Equation

The only aspect of the horizontal flow not prescribed by the source-sink field is the toroidal motion (or, alternatively, the radial vorticity). For this flow field we use the Stokes flow equation with variable viscosity

$$0 = -\nabla P + \eta \nabla^2 \underline{v} + 2\nabla \eta \cdot \dot{\underline{e}} \quad (5)$$

where P is the nonhydrostatic pressure (the hydrostatic pressure gradient having cancelled with gravitational body forces), η is dynamic viscosity, and

$$\dot{\underline{e}} = \frac{1}{2}(\nabla \underline{v} + [\nabla \underline{v}]^\dagger) \quad (6)$$

is the strain rate tensor. The fluid layer is assumed to be bounded above and below by relatively inviscid media (see *Bercovici* [1993] for discussion of this assumption). These boundaries are thus assumed free-slip and as the layer is shallow, vertical shear stresses are assumed zero across the layer; therefore, throughout the layer [*Chandrasekhar*, 1961]

$$r \frac{\partial}{\partial r} \left(\frac{v_\theta}{r} \right) = r \frac{\partial}{\partial r} \left(\frac{v_\phi}{r} \right) = 0. \quad (7)$$

This condition is used to prescribe radial derivatives of horizontal velocity and also implies that horizontal divergence D and radial vorticity

$$\omega_r = \hat{r} \cdot \nabla \times \underline{v} = -\nabla_H^2 \Psi \quad (8)$$

are independent of r . Only a single equation is necessary to determine the toroidal potential; this is the radial vorticity equation, i.e., $\underline{r} \cdot \nabla \times$ of (5). After evaluating this equation at the sphere's surface $r = R$ and nondimensionalizing ∇ and ∇_H by $1/R$; D , ω_r and $\dot{\underline{e}}$ by $D_{\max} = \max|D|$; \underline{v} by RD_{\max} ; Φ and Ψ by $R^2 D_{\max}$; and η by a reference viscosity η_o , we obtain (after some manipulation and use of (7))

$$0 = \eta(2 - L^2)L^2\Psi + \nabla_H \eta \times \nabla_H[(2 - L^2)\Phi] - \nabla_H \eta \cdot \nabla_H[(2 - L^2)\Psi] + 2\hat{r} \cdot \nabla \times (\nabla \eta \cdot \dot{\underline{e}}) \quad (9)$$

where $L^2 = -\nabla_H^2$; note that radial derivatives are eliminated through (7), leading to the factors of $L^2 - 2$. The last term on the left side of (9) can be reduced, and portions involving first order derivatives in η can be combined with the second and third terms (see the Cartesian analog of *Bercovici* [1993]). However, for computational purposes, this term is treated somewhat differently, as discussed below. Note that without horizontal variations in viscosity, (9) is a homogeneous equation in Ψ ; as the domain is naturally periodic, this would only yield a null solution in Ψ .

Rheology

Most mantle dynamic studies employing a non-Newtonian rheology use a basic pseudo-plastic, i.e., power law or Ostwald-de Waele rheology. As suggested by *Bercovici* [1993], such a rheology may not be sufficient to generate plate tectonic type flows and self-lubrication mechanisms (i.e., wherein flow resistance, not just viscosity, can decrease with added strain rate) are possibly important. (Indeed, the main purpose of this paper is to test whether this suggestion applies to realistic plate tectonic motions.) To describe both pseudo-plasticity and self-lubrication, we use a simplified form of the Carreau equation [*Bird et al.*, 1987]

$$\eta = (\gamma + \dot{\underline{e}}^2)^{\frac{1}{2}(1/n-1)} \quad (10)$$

where

$$\dot{\underline{e}}^2 = \dot{\underline{e}} : \dot{\underline{e}} = 2(D^2 + \dot{\underline{e}}_{\phi\phi}^2 + \dot{\underline{e}}_{\theta\theta}^2 - D\dot{\underline{e}}_{\phi\phi}) \quad (11)$$

is the second strain rate invariant, and the strain rate elements are

$$\dot{\underline{e}}_{\phi\phi} = \cot \theta \frac{\partial \Phi}{\partial \theta} + \frac{1}{\sin^2 \theta} \frac{\partial^2 \Phi}{\partial \phi^2} - \frac{\partial^2}{\partial \theta \partial \phi} \left(\frac{\Psi}{\sin \theta} \right) \quad (12)$$

$$\dot{\underline{e}}_{\theta\theta} = \cot \theta \frac{\partial \Psi}{\partial \theta} + \frac{1}{\sin^2 \theta} \frac{\partial^2 \Psi}{\partial \phi^2} + \frac{\partial^2}{\partial \theta \partial \phi} \left(\frac{\Phi}{\sin \theta} \right) + \frac{1}{2}L^2\Psi. \quad (13)$$

In obtaining (11), we have used the fact that the radial and colatitudinal normal strain rates are $\dot{\underline{e}}_{rr} = -D$ and $\dot{\underline{e}}_{\theta\theta} = D - \dot{\underline{e}}_{\phi\phi}$, and by (7) the vertical shear rates $\dot{\underline{e}}_{r\theta}$ and $\dot{\underline{e}}_{r\phi}$ are zero. The power law index is n , and the constant γ simply determines a maximum viscosity (i.e., precludes singularities in the viscosity field) for each n . The maximum viscosity is thus $\gamma^{\frac{1}{2}(1/n-1)}$. Since the maximum strain rate is $O(1)$, then $\max(\dot{\underline{e}}^2) \approx 2$ and thus the minimum viscosity is always approximately $(\gamma + 2)^{\frac{1}{2}(1/n-1)}$.

When $n > 0$, (10) describes the basic power law rheology; dilatancy occurs for $0 < n < 1$, Newtonian flow for $n = 1$ and pseudo-plasticity for $n > 1$. For $n < 0$, self-lubricating rheologies occur because for $\dot{\underline{e}} > \sqrt{-n\gamma}$, the flow resistance $2\eta\dot{\underline{e}}$ (actually, the square root of the second deviatoric stress invariant) decreases with increasing strain rate (Figure 1). We call the self-lubricating rheology with $n = -1$ the Whitehead-Gans (WG) rheology as it was proposed by *Whitehead and Gans* [1974] to be a continuum model of stick-slip behavior.

Figure 1 shows stress and viscosity versus strain rate for the WG and several power law rheologies. In this study we consider power law rheologies up to $n = 21$ to demonstrate asymptotic behavior. The viscosity plot in Figure 1 shows the WG and the $n = 21$ cases with γ adjusted such that they have identical maximum viscosities and similar minimum viscosities. Although these two cases have comparable viscosity contrasts, the dissimilarity between their viscosity curves plays a crucial role in the problem of plate generation.

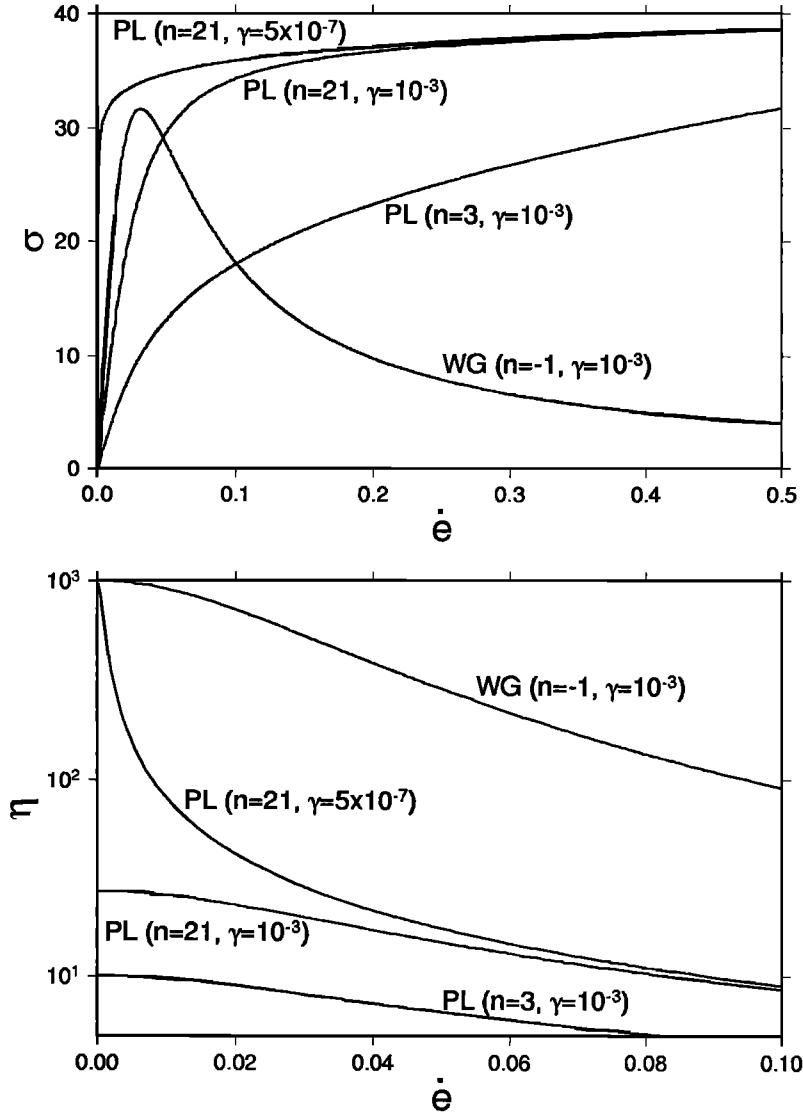


Figure 1. Constitutive relations for various rheologies. (top) Stress $\sigma = 2\eta\dot{\epsilon}$ versus strain rate $\dot{\epsilon}$ for power law (PL) and Whitehead-Gans stick-slip (WG) rheologies; stress for the power law (PL) cases are multiplied by 20. (bottom) Viscosity η versus $\dot{\epsilon}$ for the range of strain rates over which most of the viscosity variation occurs in the PL cases.

Solution Method

To solve (9), we first separate viscosity into constant and variable terms, i.e.,

$$\eta = \eta_{\max} + \eta'(\theta, \phi) \quad (14)$$

where η_{\max} is the maximum viscosity. This separation scheme has been shown to facilitate numerical stability [Christensen and Harder, 1991]. An approximate solution to (9) is obtained with a spectral transform technique similar to that of Glatzmaier [1984]. D , ω_r , Φ , Ψ , and η' are represented by spherical harmonic series; i.e.,

$$(D, \omega_r, \Phi, \Psi, \eta') = \sum_{l=0}^{\infty} \sum_{m=-l}^{+l} (D_l^m, \omega_l^m, \Phi_l^m, \Psi_l^m, \eta_l^m) Y_l^m(\theta, \phi) \quad (15)$$

where Y_l^m is a normalized spherical harmonic function of degree l and order m and $D_l^m, \omega_l^m, \Phi_l^m, \Psi_l^m$ and η_l^m are the spherical harmonic transforms of D, ω_r, Φ, Ψ and η' . By definition of a spherical harmonic, $L^2 Y_l^m = l(l+1) Y_l^m$. The toroidal equation (9) can thus be transformed to

$$\begin{aligned} \eta_{\max} (l(l+1) - 2) l(l+1) \Psi_l^m = & \int_0^{2\pi} \int_{-1}^{+1} \left\{ \eta' (2 - L^2) L^2 \Psi \right. \\ & + \nabla_H \eta' \times \nabla_H [(2 - L^2) \Phi] - \nabla_H \eta' \cdot \nabla_H [(2 - L^2) \Psi] \\ & \left. + 2\hat{r} \cdot \nabla \times (\nabla \eta' \cdot \dot{\epsilon}) \right\} Y_l^{m*} d(\cos \theta) d\phi \quad (16) \end{aligned}$$

from which each Ψ_l^m can be solved algebraically. The right side of (16) is evaluated by fast Fourier transforms and Gaussian quadrature [Glatzmaier, 1984]. Equation (16) could also be solved with a purely spectral-Galerkin approach using Wigner-3j or Clebsch-Gordan symbols

[see *Ribe*, 1992]; however, there is no apparent computational advantage to this technique especially since viscosity itself is a nonlinear (usually irrational) function of the flow field and thus the strain rate elements and viscosity must be calculated in the physical (θ, ϕ) domain.

The calculation of the nonlinear terms on the right side of (16) deserves some discussion. The spectral representation is used to facilitate evaluation of derivatives; e.g., $L^2\Psi = \sum_{lm} l(l+1)\Psi_l^m Y_l^m$. Derivatives in ϕ are straightforward (e.g., $\partial\eta'/\partial\phi = \sum_{lm} im\eta_l^m Y_l^m$) and for derivatives in θ we use the recursion relation [see *Washington and Parkinson*, 1986]

$$\sin\theta \frac{\partial Y_l^m}{\partial\theta} = l\epsilon_{l+1}^m Y_{l+1}^m - (l+1)\epsilon_l^m Y_{l-1}^m \quad (17)$$

where

$$\epsilon_l^m = \sqrt{\frac{l^2 - m^2}{4l^2 - 1}}. \quad (18)$$

The fourth term of the integrand on the right side of (16) requires a slightly more elaborate treatment [*Glatzmaier*, 1984]. We express this term as

$$2\hat{r} \cdot \nabla \times (\nabla\eta' \cdot \hat{e}) = \frac{1}{\sin\theta} \frac{\partial}{\partial\theta} (\sin^2\theta g) - \frac{\partial f}{\partial\phi} \quad (19)$$

where

$$(g, f) = \frac{2}{\sin\theta} \left[\frac{\partial\eta'}{\partial\theta} (\dot{e}_{\theta\phi}, D - \dot{e}_{\phi\phi}) + \frac{1}{\sin\theta} \frac{\partial\eta'}{\partial\phi} (\dot{e}_{\phi\phi}, \dot{e}_{\theta\phi}) \right]. \quad (20)$$

Given the recursion relation (17), then

$$\int_0^{2\pi} \int_{-1}^{+1} 2\hat{r} \cdot \nabla \times (\nabla\eta' \cdot \hat{e}) Y_l^{m*} d(\cos\theta) d\phi = (l+1)\epsilon_l^m g_{l-1}^m - l\epsilon_{l+1}^m g_{l+1}^m - imf_l^m \quad (21)$$

where g_l^m and f_l^m are the spherical harmonic transforms of f and g .

Equation (16) is solved iteratively until Ψ achieves reasonable convergence. The convergence error is

$$\epsilon = \frac{\sum_{lm} |\Psi_l^{m(j)} - \Psi_l^{m(j-1)}|^2}{\sum_{lm} |\Psi_l^{m(j)}|^2} \quad (22)$$

where j implies the iteration number. Convergence is assumed when ϵ reaches a number which is $\ll 1$. For cases with relatively low viscosity contrasts between weak and strong fluid, convergence is readily attained with $\epsilon < 10^{-7}$. However, for cases with large viscosity contrasts (of order 1000), convergence is more difficult to achieve and the minimum ϵ is as much as $O(10^{-5})$. Thus the high viscosity contrast cases must be interpreted with some caution. The minimum value of ϵ will be denoted in the captions to relevant figures.

Net Lithospheric Rotation

It is important to note that the solutions to (16) for the spherically symmetric toroidal mode ($l = 0$) and the net rotation modes ($l = 1$) are indeterminate. The spherically symmetric mode is indeed meaningless. The net rotation modes clearly cannot appear in terms proportional to $L^2 - 2$ (or $l(l+1) - 2$) and cannot contribute to any of the strain rate elements, and hence have no effect on viscosity (as expected). Thus net rotation cannot be obtained with this model, suggesting that horizontal normal stresses in the lithosphere, such as ridge-push or slab-pull (which the source-sink formulation essentially models, kinematically), cannot generate net lithospheric motion. This supports the hypothesis that net rotation comes from underlying mantle tractions [*O'Connell et al.*, 1991; *Ricard et al.*, 1991].

Regardless of physical implications for the lack of net rotation in the model, we are still forced to assume a no-net-rotation frame of reference. Indeed, the rate of net rotation in Earth's lithosphere is reference frame dependent; hence its relevance is unclear. It has been suggested that the no-net-rotation frame is a viable reference frame [*Minster et al.*, 1974; *Lithgow-Bertelloni et al.*, 1993], though it does tend to artificially remove much of the spin vorticity extant in large plates (especially the Pacific) [*Bercovici and Wessel*, 1994]. Here we adopt the no-net-rotation frame out of necessity; we can only state that it is a physically plausible frame but that suggestions about the importance of net rotation are by no means implied.

Results

In this section we examine model results (arising from the solution of the toroidal equation (9)) for various source-sink fields and rheologies. In each case the source-sink field is $D = \nabla_H \cdot \tilde{u}$, where $\tilde{u}(\theta, \phi)$ is the velocity field of a plate motion model. We examine two plate models: one for an idealized rectangular plate, the other for Earth's present-day plates. In each case the radial vorticity of the plate model $\tilde{\omega}_r = \hat{r} \cdot \nabla \times \tilde{u}$ is known. Our qualitative diagnostics are (1) the fluid velocity field (compared to the plate velocity field), (2) the fluid vorticity field $\omega_r = L^2\Psi$ (compared to the plate vorticity $\tilde{\omega}_r$), and (3) the fluid viscosity field η . Our quantitative diagnostics are the toroidal-poloidal kinetic energy ratio

$$KE_T/KE_P = \frac{\sum_{lm} l(l+1)|\Psi_l^m|^2}{\sum_{lm} l(l+1)|\Phi_l^m|^2} \quad (23)$$

(where kinetic energy is essentially used here as a mean-square velocity) and vorticity deviation (or mean-square misfit)

$$\Omega = \frac{\sum_{lm} |\omega_l^m - \tilde{\omega}_l^m|^2}{\sum_{lm} |\tilde{\omega}_l^m|^2}. \quad (24)$$

The kinetic energy ratio KE_T/KE_P measures energy partitioning between toroidal and poloidal flow fields

($KE_T/KE_P = 1$ indicates equipartitioning). The vorticity deviation contains both a comparison of the net power in the vorticity fields ω_r and $\tilde{\omega}_r$, as well as the spatial correlation between each field. The success of the fluid model lies in its ability to reproduce the plate model's kinetic energy ratio

$$\widetilde{KE_T}/KE_P = \frac{\sum_{lm} \frac{1}{l(l+1)} |\tilde{\omega}_l^m|^2}{\sum_{lm} l(l+1) |\Phi_l^m|^2} \quad (25)$$

and to generate a small Ω (e.g., $\Omega = 0$ implies perfect reproduction of the original plate model). In all cases, comparisons to the plate model velocity and vorticity fields are in a no-net-rotation reference frame.

All the numerical solutions presented here are calculated with the spherical-harmonic series truncated at $l_{\max} = 170$; the physical grid (on which nonlinear terms are calculated and transformed) correspondingly has 512 longitudinal by 256 colatitudinal grid points. (The relation between l_{\max} and the number of grid points is prescribed to reduce aliasing effects; see *Glatzmaier* [1984].) The adequacy of the numerical resolution is tested by examining KE_T/KE_P and Ω as l_{\max} increases (for $85 \leq l_{\max} \leq 255$) for the most non-Newtonian solutions (in particular, the WG and $n = 21$ power law rheologies) and both plate models; these quantities are sufficiently independent of truncation at $l_{\max} = 170$ to insure adequate numerical resolution. Power spectra for the numerical solutions are also examined and are found to fall off between 7 and 8 orders of magnitude, also indicating that the solutions are well resolved (see below).

Idealized Plate Motions

The model presented in this paper employs continuum theory and hence requires a continuous (or more specifically an analytically differentiable) source-sink field D . As in the work by *Bercovici* [1993] and *Bercovici and Wessel* [1994], we represent plate geometries with analytically continuous shape functions. The velocity field of a single moving plate is

$$\tilde{\mathbf{v}} = \mathbf{W} \times \mathbf{R}S(\theta, \phi) \quad (26)$$

where \mathbf{W} is the angular velocity vector of the plate about its Euler pole and \mathbf{R} is the position vector of a point on the plate. The function S is the shape function of the plate; it is 1 inside the plate, 0 far outside the plate, and transitions smoothly from 1 to 0 at the plate margins. In this subsection we simply use the “rectangular” plate geometry of *Bercovici and Wessel* [1994] in which $\mathbf{W} = W\hat{z}$ (where \hat{z} points from the sphere's center to the north geographic pole), $\mathbf{R} = \hat{r}$, and

$$S = s(\theta, \frac{\pi}{2}, \beta, \delta) s(\phi, \pi, \frac{\beta}{\cos \beta}, \delta) \quad (27)$$

where

$$s(x, x_0, b, d) = \frac{\tanh\left(\frac{x-x_0+b}{d}\right) - \tanh\left(\frac{x-x_0-b}{d}\right)}{2 \tanh(b/d)}. \quad (28)$$

The parameter β is the plate half width in the latitudinal direction; to make the plate “square” (i.e., have margins of equal arc length) the half width in the longitudinal direction is $\beta/\cos \beta$. The parameter δ is the plate margin half width. The angular speed of the plate W is chosen such that the maximum D is unity. This idealized plate model is constructed so that each plate edge is uniquely identified with either toroidal or poloidal motion.

Figure 2 shows velocity ($\tilde{\mathbf{v}}$), horizontal divergence (D) (i.e., the source-sink function) and radial vorticity ($\tilde{\omega}_r$) for this plate model with particular choices of β and δ . The background flow opposite to the plate motion appears because the velocity is shown in a no-net-rotation frame of reference. It is worth noting that even though the plate is contrived to be “square”, the maximum vor-

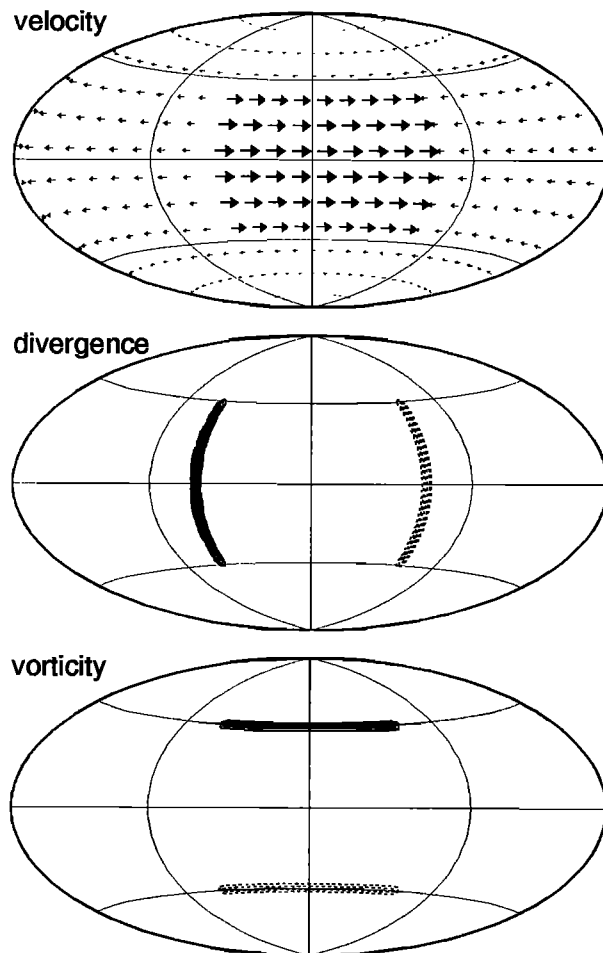


Figure 2. Velocity, horizontal divergence, and radial vorticity for the “square” plate model with $\beta = 45^\circ$ and $\delta = 2^\circ$. The maximum dimensionless velocity is 0.0514; minimum and maximum divergence are ± 1 ; minimum and maximum vorticity are ± 0.7425 . Contour interval for both divergence and vorticity is 0.3

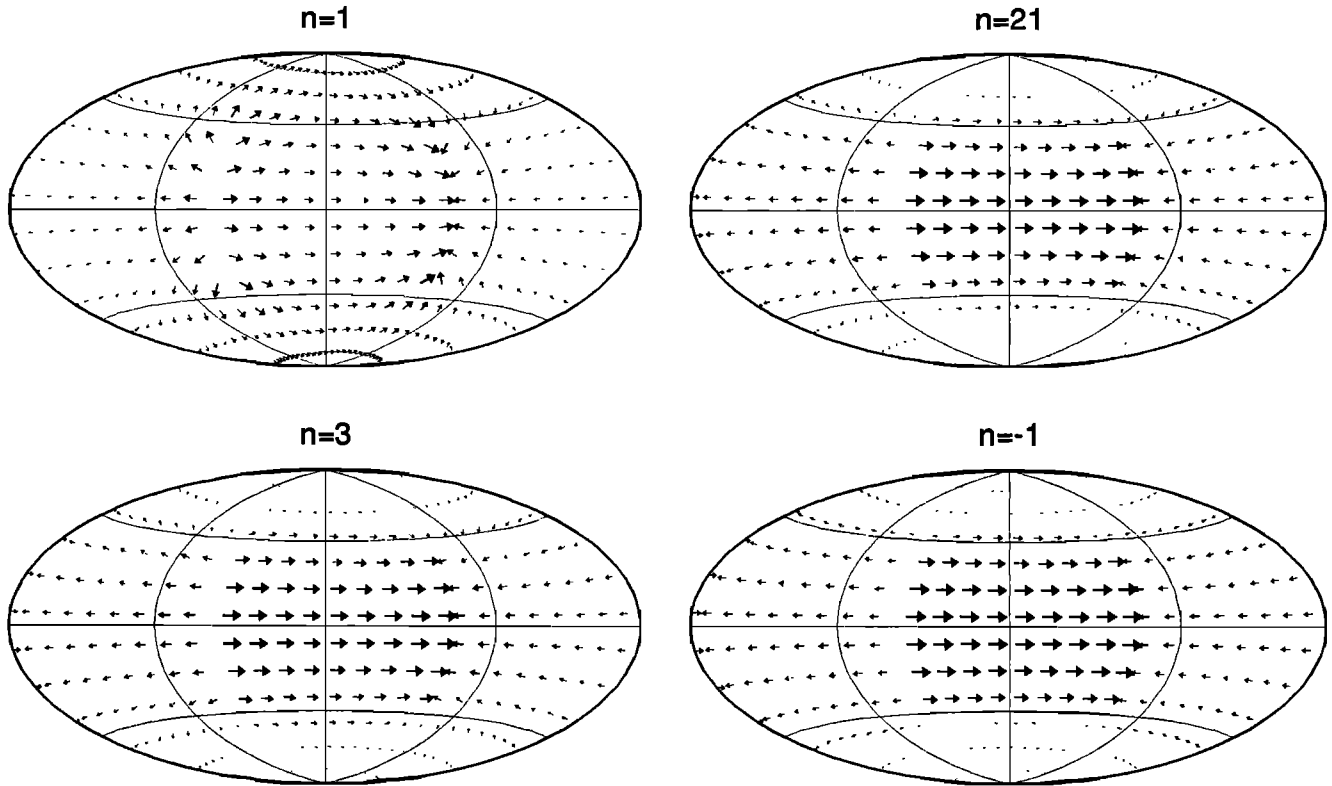


Figure 3. Velocity fields for various non-Newtonian flows driven by the source-sink field (i.e., the horizontal divergence) from Figure 2. Power law indices are indicated. All cases are for $\gamma = 10^{-3}$. The maximum velocity for the $n = 1, 3, 21,$ and -1 cases are 0.0415, 0.0430, 0.0441, and 0.0470, respectively. The minimum values of the convergence error ϵ for the Newtonian and the power law cases ($n \geq 1$) shown are less than 10^{-7} ; for the WG case ($n = -1$) the $\min(\epsilon) = 6.5 \times 10^{-6}$.

ticity is significantly less than the maximum divergence, unlike that of a square plate in a Cartesian geometry [see *Olson and Bercovici, 1991; Bercovici and Wessel, 1994*].

Velocity. The velocity fields (\underline{v}) for a few non-Newtonian flows are shown in Figure 3; these sample the full range of power-law indices, from Newtonian ($n = 1$), to mantle-like ($n = 3$) to extreme ($n = 21$). Also displayed is the flow field with the WG stick-slip rheology ($n = -1$). In the cases shown, $\gamma = 10^{-3}$, yielding a high-viscosity contrast for $n = -1$, but not for the power law cases. High viscosity contrast power law cases are discussed later.

The most dramatic difference in velocity occurs between the purely irrotational Newtonian flow field and the non-Newtonian fields; differences amongst the non-Newtonian flow fields are in fact fairly subtle. The maximum velocity occurs for the WG ($n = -1$) case and is 91% of the maximum \bar{v} ; yet this maximum is not so different from the other fluid dynamical cases (even the Newtonian one has a maximum velocity which is 81% of the maximum \bar{v}). Some of the subtle qualitative differences between the WG and the power law cases are worth noting. The contrast between the background and plate flow across the convergent zones is slightly more noticeable in the WG case than elsewhere; how-

ever, the contrast across the strike-slip margins appears fairly equal amongst all cases. Most notable is that the source and sink maintain dipolar flow (i.e., monopolar divergence or convergence at the corners of the plate) for the power law cases, even up to $n = 21$; however, the dipole effect is largely eliminated in the WG case.

Radial vorticity. Figure 4 shows radial vorticity ω_r for the same non-Newtonian cases as in Figure 3 ($\omega_r = 0$ for the Newtonian case). There is little difference in vorticity between the two power-law cases ($n = 3$ and $n = 21$) in either the shape of the field or amplitude (the $n = 21$ vorticity field has slightly larger extrema). The WG ($n = -1$) rheology is quite distinct from the power-law cases, producing narrower, more intense bands of vorticity (or strike-slip shear) reminiscent of the original plate's vorticity (see Figure 2). The extrema for all three cases occur at the corners of the plate (or ends of the source and sink), however the WG case maintains some additionally complex structure which acts to eliminate dipolar flow at the corners. The maximum ω_r for the WG rheology is 50% greater than that of the $n = 21$ case, though even the WG maximum vorticity is only 40% of the maximum $\bar{\omega}_r$.

Viscosity. Figure 5 displays the viscosity fields for the same non-Newtonian cases as in Figures 3 and 4. Shading is used to indicate the viscosity lows or the

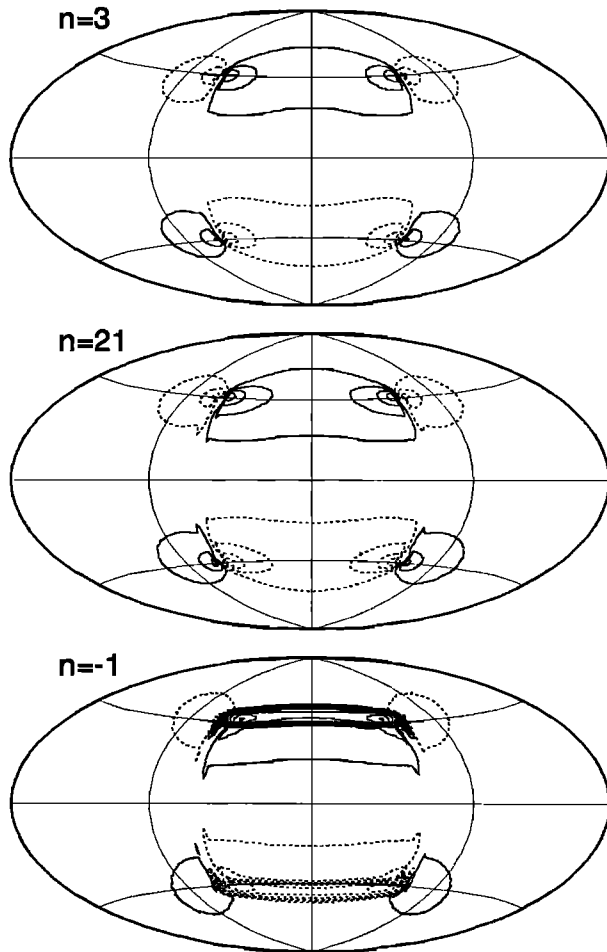


Figure 4. Radial vorticity fields for the three non-Newtonian cases of Figure 3. All three cases are shown with the same contour interval of 0.038. The minimum and maximum vorticities for the $n = 3$, 21, and -1 cases are ± 0.1488 , ± 0.1774 , and ± 0.2687 , respectively. Convergence errors are discussed in Figure 3.

weak pseudo-margins. All rheologies show deep viscosity lows over the source and sink since the strain rates there are largely prescribed. However, the viscosity lows along the strike-slip margins vary considerably between the different rheologies. The power law cases have relatively shallow viscosity lows, and in the case of $n = 3$, they are not actually contiguous along the strike-slip margin. The viscosity low in the WG case is contiguous and almost constant around the entire plate margin, for strike-slip as well as divergent-convergent zones. Finally, the WG rheology produces the most constant viscosity highs and lows and the sharpest viscosity gradients at the margins (even for the source and sink regions).

High viscosity contrast power law cases. To determine whether the results so far are more indicative of prescribed viscosity contrast than choice of rheology, we examine power law cases ($n \geq 1$) with $\gamma = 5 \times 10^{-7}$. With this γ , the viscosity contrast at the highest power law index ($n = 21$) is comparable to that for the WG

($n = -1$) case with $\gamma = 10^{-3}$. Figure 6 shows velocity, vorticity, and viscosity for the solutions with $n = 5$ and $n = 21$. (The $n = 5$ case is shown as it yields relatively high and low values of KE_T/KE_P and Ω , respectively, as discussed in the next section.) Both cases appear less platelike than any of the previous calculations. The velocity fields are not significantly different from the other cases (though clearly velocity is not a very precise diagnostic). Their vorticity fields, however, are fairly diffuse, do not have any narrow extrema (even at the plate corners), and are more distributed throughout the background material (i.e., outside the original plate) than other cases. The viscosity fields show the largest deviation from the previous cases; viscosity lows are very broad, while viscosity highs are relatively narrow and small, even in the region of the original plate. This behavior is, in fact, to be expected. Figure 1 shows how, for $n = 21$, η stays of the order of 10 down to very low strain rates for either $\gamma = 10^{-3}$ or $\gamma = 5 \times 10^{-7}$. The viscosity for $\gamma = 5 \times 10^{-7}$ only exceeds 100 for $\dot{\epsilon} < 0.01$, while the entire range of $\dot{\epsilon}$ is between 0 and $O(1)$. Thus, even though the case with $\gamma = 5 \times 10^{-7}$ yields large viscosity contrasts, the high viscosities are only attained for a very narrow range of strain rates. Low viscosities therefore occur for the majority of strain rates; thus most of the fluid (instead of just the narrow margins) is weak. (This phenomenon also relates to the “plateness” regimes mapped out by *Weinstein and Olson* [1992]). In contrast, the WG rheology obtains high viscosities for $\dot{\epsilon} < 0.5$, and thus a sizeable portion of the fluid layer is strong. This exercise suggests that the differences between the power law and WG rheologies observed so far are not simply due to different viscosity contrasts.

Kinetic energy partitioning and vorticity deviation. Figure 7a shows the toroidal-poloidal kinetic energy ratio KE_T/KE_P (see (23)) and vorticity deviation Ω (see (24)) versus n . For $n \geq 1$, curves for both $\gamma = 10^{-3}$ and $\gamma = 5 \times 10^{-7}$ are shown; the values for the WG case are also shown for comparison. The kinetic energy ratio for the plate model is $\widetilde{KE_T/KE_P} = 0.72$. The maximum KE_T/KE_P and minimum Ω are achieved by the WG case. The power law rheology with $\gamma = 5 \times 10^{-7}$ and small n , however, yields values of KE_T/KE_P and Ω comparable to those of the WG case, even though it produces the least platelike flow and viscosity fields (see previous subsection and Figure 6). For the power law rheologies, KE_T/KE_P and Ω appear to approach asymptotic values with increasing n . With $\gamma = 5 \times 10^{-7}$, an increase in n actually yields a decrease in KE_T/KE_P and an increase in Ω , i.e., an adverse effect on the generation of platelike toroidal flow.

Figure 7b shows KE_T/KE_P and Ω versus γ for the WG ($n = -1$) rheology. The most platelike toroidal fields are clearly obtained for $\gamma < 10^{-2}$. This occurs because the maximum strain rate in the fluid must be significantly greater than the cutoff strain rate of $\sqrt{-n\gamma}$

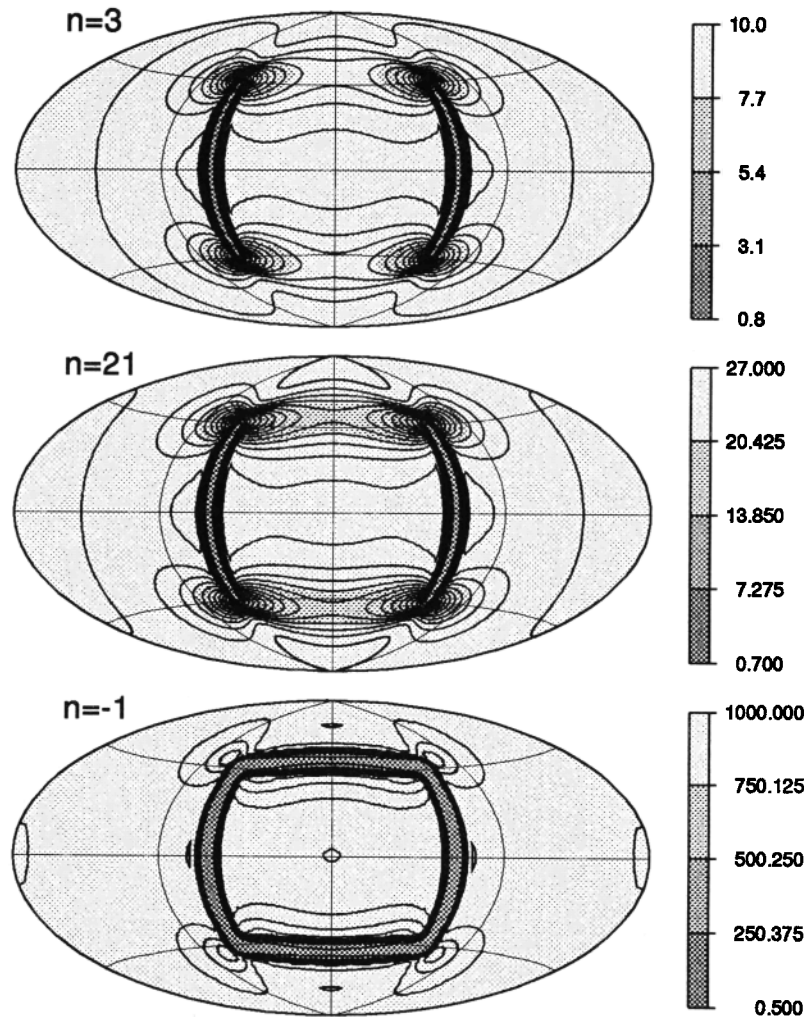


Figure 5. Viscosity fields for the three non-Newtonian cases of Figures 3 and 4. Shading is included to display viscosity lows and highs; minimum and maximum viscosities are thus indicated on the gray-scale bars. The contour interval for the $n = 3$, 21, and -1 cases are 1.22, 1.75, and 66.63, respectively.

for the flow to become platelike; otherwise, the margins are not sufficiently weak.

On the whole, the best quantitative reproduction of the original plate's toroidal field is attained by the WG case with sufficiently small γ , although the power law rheology (with very small γ) yields comparable results at moderately small n . Neither case, however, is close to yielding ideal results, particularly with respect to Ω (which ideally would be 0). More desirable values of KE_T/KE_P and Ω might be obtained with the WG rheology and $\gamma < 10^{-4}$, but this is presently beyond the capability of the numerical model(er).

Present-Day Plate Tectonic Motions

Classical plate tectonic theory describes motions at Earth's surface in terms of independently moving rigid bodies [Morgan, 1968; Minster and Jordan, 1978; DeMets *et al.*, 1990]. This yields discontinuous changes in velocity at plate margins, and thus the surface di-

vergence D and vorticity $\bar{\omega}_r$ of such a model are singularities. In the source-sink model, D must be at least second-order differentiable. Thus classical plate tectonic theory cannot be directly applied to our continuum model. In fact, Earth's tectonic plates are not discontinuous; i.e., intraplate deformation is significant and plate margins have some finite width. Some refinement of the plate tectonic model to account for margin widths (even crudely) is therefore required for this study. We thus use the analytically continuous plate model of Bercovici and Wessel [1994]. In short, this plate model smooths the boundaries of the present-day plates and describes each plate's shape and margin thickness with analytically continuous functions analogous to (28). Plate 1 shows divergence D and vorticity $\bar{\omega}_r$ for this plate model in the no-net-rotation reference frame (i.e., the $l = 1$ modes of the vorticity are removed). As can be seen, the model captures the basic character of the present-day plates, though it tends to

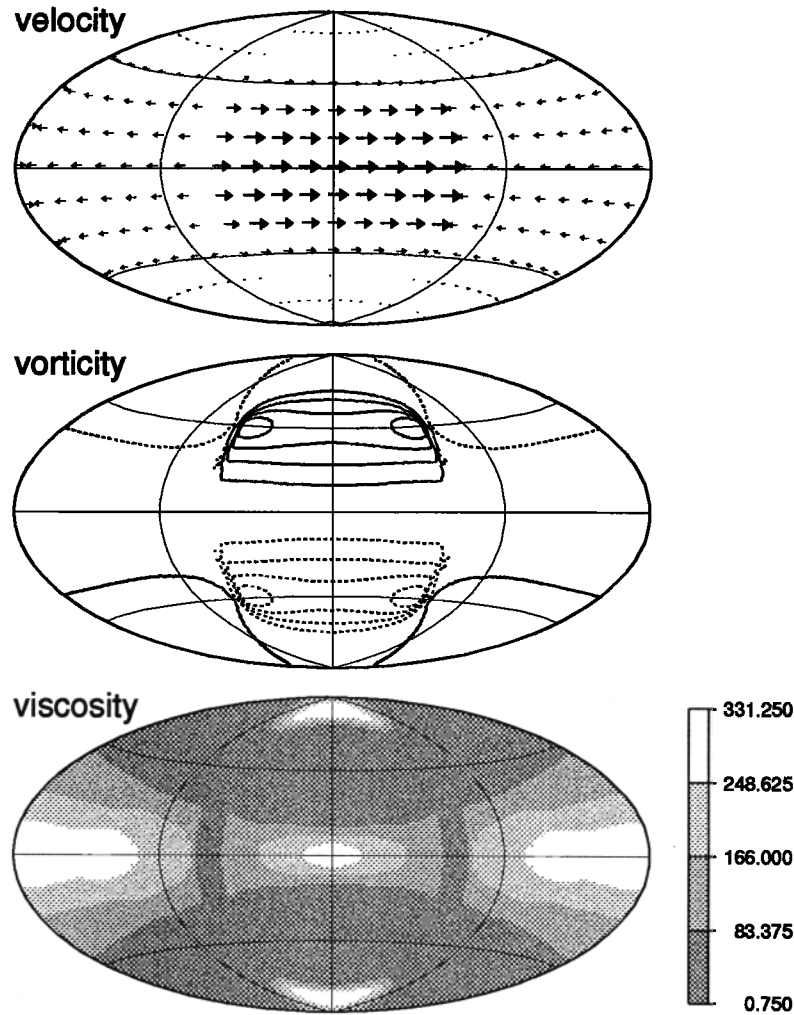


Figure 6a. Velocity, vorticity and viscosity for the high viscosity contrast power law cases (i.e., $\gamma = 5 \times 10^{-7}$) with $n = 5$. The maximum velocity is 0.0475. Minimum and maximum vorticities are ± 0.1330 , vorticity contour interval is 0.027, and convergence error ϵ is 2×10^{-6} .

reduce the curvature of plate boundaries. Velocity is not shown in this or subsequent figures; as the Philippine plate tends to overwhelm the velocity scale, the velocity fields are not particularly enlightening. Both the divergence and vorticity fields are normalized by the maximum D (the value of which is shown). Notice the minimum (negative) vorticity (corresponding to right-lateral strike-slip) is slightly less in magnitude than the vorticity maximum. This is primarily due to the fact that the eastern boundary of the Philippine plate is closer to the plate's Euler pole.

The following non-Newtonian flow solutions are only for $\gamma = 10^{-3}$. Higher viscosity contrast cases (i.e., with much smaller γ) were not obtainable with satisfactory convergence.

Radial vorticity. Plate 2 displays ω_r for the same three rheologies of Figure 4. The largest vorticity is generated by the $n = 21$ case. However, both power law

rheologies underestimate the minimum vorticity, leading to the blue shift in their vorticity fields (i.e., the zero, background vorticity is shifted off the center gray shade into the blue end of the color scale). The ratio of the magnitudes of the minimum and maximum ω_r for both $n = 3$ and $n = 21$ is approximately 1/2. In contrast, the original plate has a ratio of 0.89. The WG rheology generates vorticity extrema with approximately only 50% of the original plate's magnitudes. However, it produces more negative vorticity (right-lateral slip) than the other rheologies and yields a more proportionate distribution. The vorticity field has little if any blue shifting, and the ratio of the magnitudes of the minimum and maximum ω_r is 0.87, very close to that of the original plate model. However, the minimum and maximum vorticities primarily occur along the Philippine plate. Vorticity at other plate boundaries seems to be underestimated by the power law rheologies and

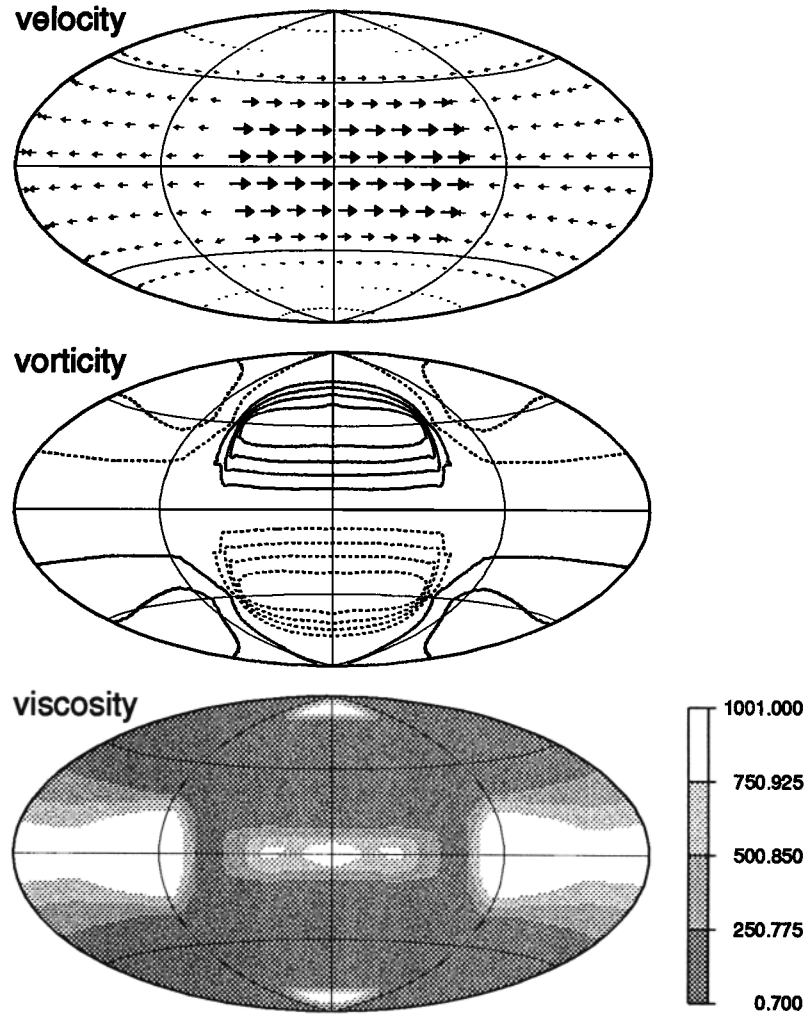


Figure 6b. Same as Figure 6a, except for $n = 21$. The maximum velocity is 0.0475. Minimum and maximum vorticities are ± 0.0947 , vorticity contour interval is 0.019, and $\epsilon = 8.4 \times 10^{-6}$.

over estimated by the WG rheology with respect to the vorticity at the Philippine plate. Nevertheless, the WG rheology appears to succeed best at producing the more subtle strike-slip zones, such as at the South-West Indian Ridge and the Romanche Fracture Zone (in the central Atlantic).

Viscosity. Viscosity fields for the three cases of Plate 2 are shown in Plate 3. The structure of the viscosity lows is largely controlled by the divergence field. The only large boundary that has significant vorticity without also having a great deal of divergence is the San Andreas fault (see Plate 1). Thus the deformation rate at most of the plate margins is essentially prescribed by the source-sink field. At the San Andreas fault, however, the existence of a weak margin is dependent almost exclusively on the generation of vorticity. The power law rheologies appear to fail at creating a significant viscosity low at this boundary (the viscosity there is not even very low, being closer to the maximum viscosity than the minimum). Thus the Pacific plate

boundary is not closed with these rheologies. The WG rheology succeeds in generating a viscosity low at San Andreas, though the viscosity there is not the minimum possible value; even so, the Pacific plate boundary appears closed. The WG rheology is also more successful at generating weak margins at the South-West Indian Ridge and the Romanche Fracture Zone and thus more efficiently closes the Antarctic plate boundary and allows the Mid-Atlantic Ridge to be contiguous. None of the rheologies are very successful at closing the South American, African, and Arabian plates, all primarily slow moving plates.

An important feature of the viscosity fields is the viscosity gradients near margins. The power law rheology allows weakening of material well outside of plate margins; this is especially noticeable on the ocean side of the Marianas trench and across South-East Asia and Indonesia. These weak zones do not correspond to any regions of intraplate deformation and are thus not necessarily desirable features. In contrast, the WG rheol-

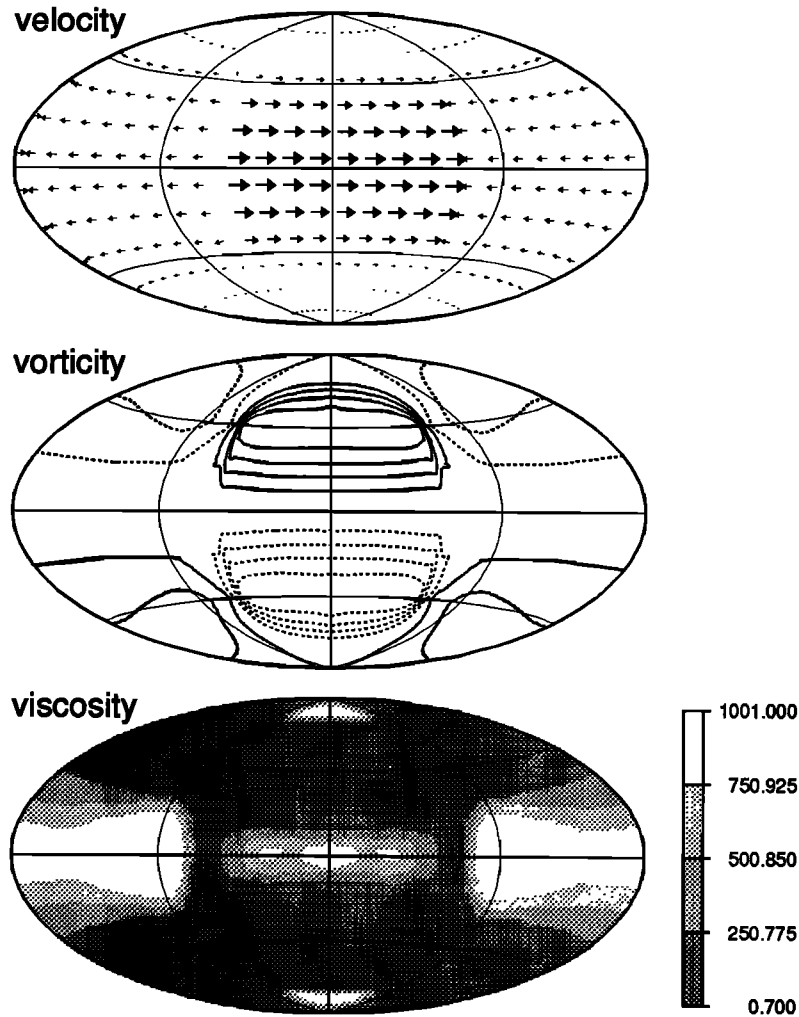


Figure 6b. Same as Figure 6a, except for $n = 21$. The maximum velocity is 0.0475. Minimum and maximum vorticities are ± 0.0947 , vorticity contour interval is 0.019, and $\epsilon = 8.4 \times 10^{-6}$.

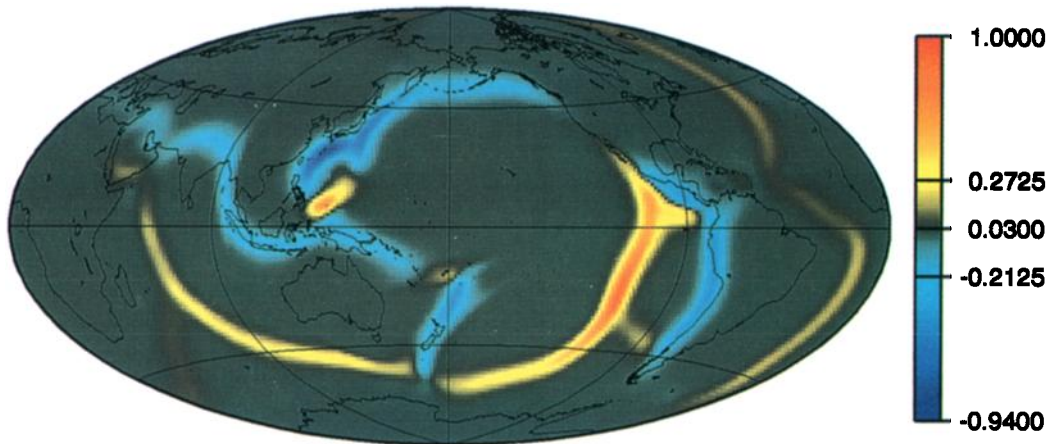
over estimated by the WG rheology with respect to the vorticity at the Philippine plate. Nevertheless, the WG rheology appears to succeed best at producing the more subtle strike-slip zones, such as at the South-West Indian Ridge and the Romanche Fracture Zone (in the central Atlantic).

Viscosity. Viscosity fields for the three cases of Plate 2 are shown in Plate 3. The structure of the viscosity lows is largely controlled by the divergence field. The only large boundary that has significant vorticity without also having a great deal of divergence is the San Andreas fault (see Plate 1). Thus the deformation rate at most of the plate margins is essentially prescribed by the source-sink field. At the San Andreas fault, however, the existence of a weak margin is dependent almost exclusively on the generation of vorticity. The power law rheologies appear to fail at creating a significant viscosity low at this boundary (the viscosity there is not even very low, being closer to the maximum viscosity than the minimum). Thus the Pacific plate

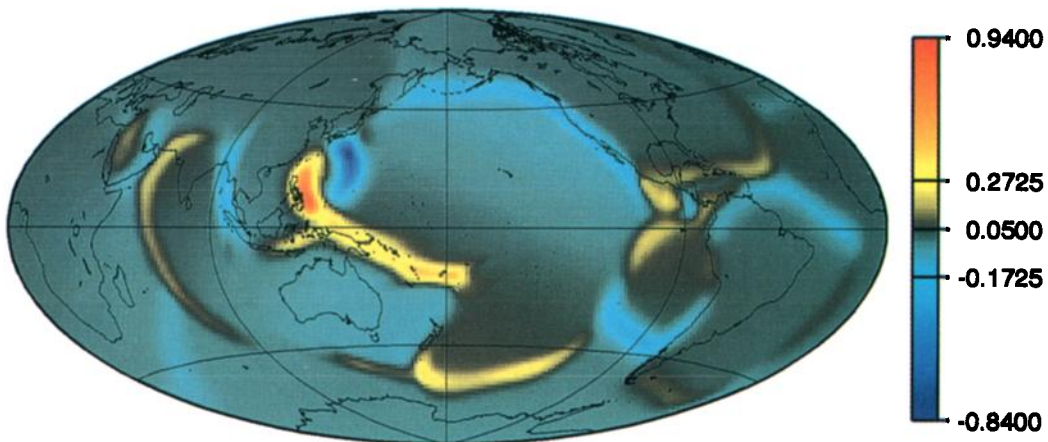
boundary is not closed with these rheologies. The WG rheology succeeds in generating a viscosity low at San Andreas, though the viscosity there is not the minimum possible value; even so, the Pacific plate boundary appears closed. The WG rheology is also more successful at generating weak margins at the South-West Indian Ridge and the Romanche Fracture Zone and thus more efficiently closes the Antarctic plate boundary and allows the Mid-Atlantic Ridge to be contiguous. None of the rheologies are very successful at closing the South American, African, and Arabian plates, all primarily slow moving plates.

An important feature of the viscosity fields is the viscosity gradients near margins. The power law rheology allows weakening of material well outside of plate margins; this is especially noticeable on the ocean side of the Marianas trench and across South-East Asia and Indonesia. These weak zones do not correspond to any regions of intraplate deformation and are thus not necessarily desirable features. In contrast, the WG rheol-

Divergence



Vorticity



normalized by
 $D_{\max} = 247.68 \text{ Gyr}^{-1}$

Plate 1. Horizontal divergence D and radial vorticity $\tilde{\omega}_r$ for the analytically continuous plate model of *Bercovici and Wessel* [1994]. The plate margins are specified to have a uniform 400 km half width. This half width gives the best truncation error in the spherical harmonic representation of the plate's divergence and vorticity [*Bercovici and Wessel*, 1994]. The color scale is stretched to enhance structure about the extrema.

power law (at large n) and WG cases, though the value associate with the WG rheology is slightly smaller. As implied by the idealized model and by *Bercovici* [1993], all power law cases appear to reach an asymptotic limit in how well they can produce tectonic plates.

Kinetic energy power spectra. The spherical harmonic power spectra of the plate tectonic toroidal and poloidal kinetic energies have been well studied [e.g., *Hager and O'Connell*, 1978, 1979, 1981; *O'Connell et al.*, 1991; *Lithgow-Bertelloni et al.*, 1993] and are known to have distinct features at low spherical harmonic degrees. The power spectra for the plate model

(which, although simplified, has very nearly the same power spectra as the discontinuous plate model; see *Bercovici and Wessel* [1994]) and the non-Newtonian flow models are shown in Figure 9. For the flow models, the toroidal energy is largest for the WG rheology at most l , followed sequentially by the $n = 21$ and $n = 3$ cases; all three non-Newtonian solutions, however, have less toroidal energy than the plate model. The spectra for the three non-Newtonian cases mirror the plates' toroidal energy spectrum reasonably well (to $l = 20$), with some exceptions. The power law rheologies do not have a local maximum at $l = 2$, nor a local minimum at

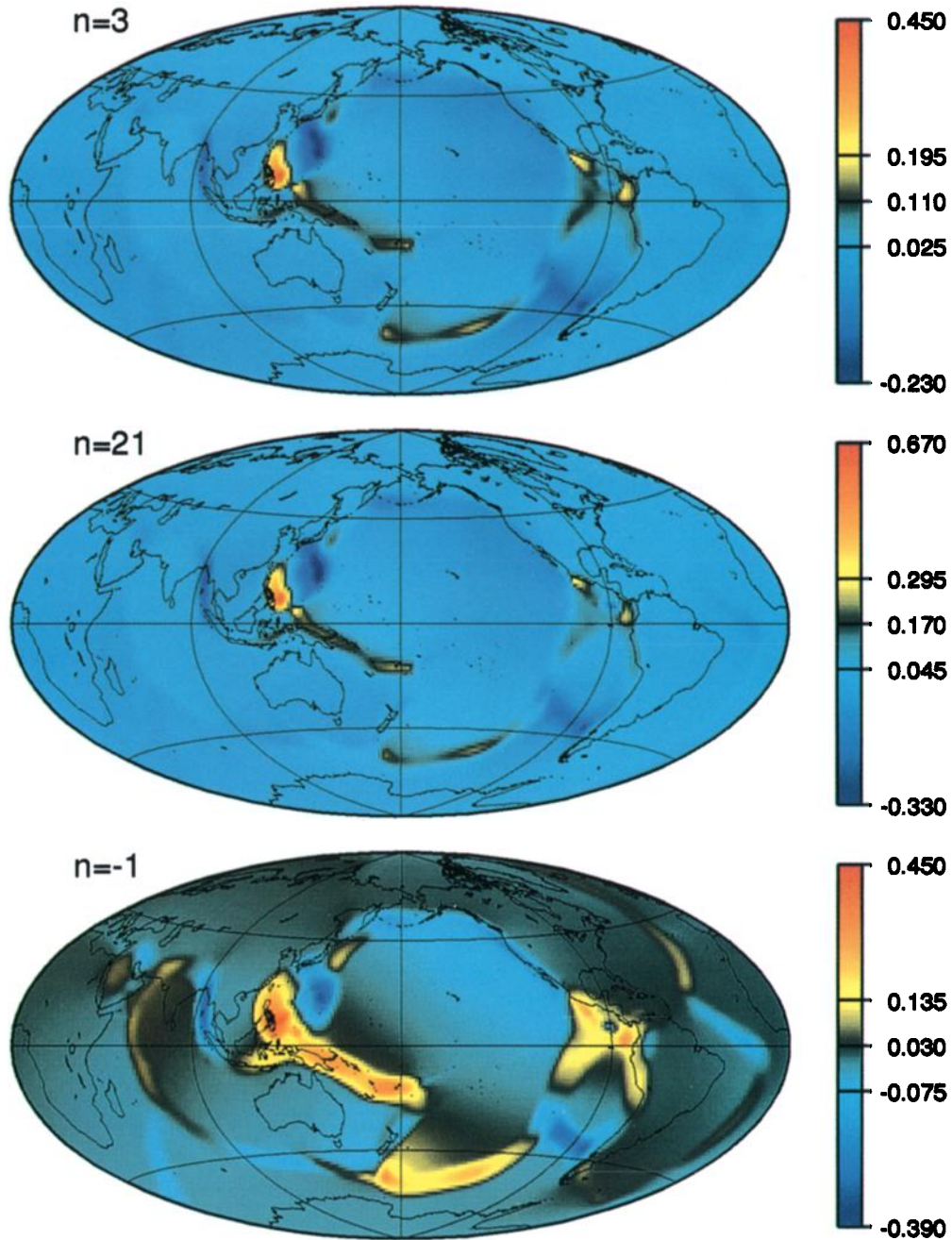


Plate 2. Radial vorticity ω_r for three non-Newtonian flows driven by the divergence (i.e., source-sink) field D from Plate 1. For all cases, $\gamma = 10^{-3}$. The convergence error for the power law cases is $\epsilon \leq 10^{-7}$, while for the WG ($n = -1$) case, $\epsilon = 2.6 \times 10^{-5}$. The color scale is stretched to enhance structure about the extrema.

$l = 4$ (which is one of the more prominent features of the plate model's spectrum). While the WG rheology does produce these features, the minimum at $l = 4$ is more subtle than that of the plate model.

Conclusions

“Plateness” Versus Toroidal Flow

In their study of two-dimensional non-Newtonian mantle convection, *Weinstein and Olson* [1992] introduced

the quantity “plateness”. Plateness measures the shape of a plate's velocity distribution: if it has steplike transitions in velocity, then its plateness is unity, while a smooth sinusoidal transition leads to null plateness. An alternative but equally viable “plateness” criterion would measure the sharpness of transitions in viscosity or strength. Clearly, plateness is a desirable aspect of a plate tectonic type flow. However, the results of this study indicate that plateness is possibly independent of the magnitude of toroidal motion, another necessary

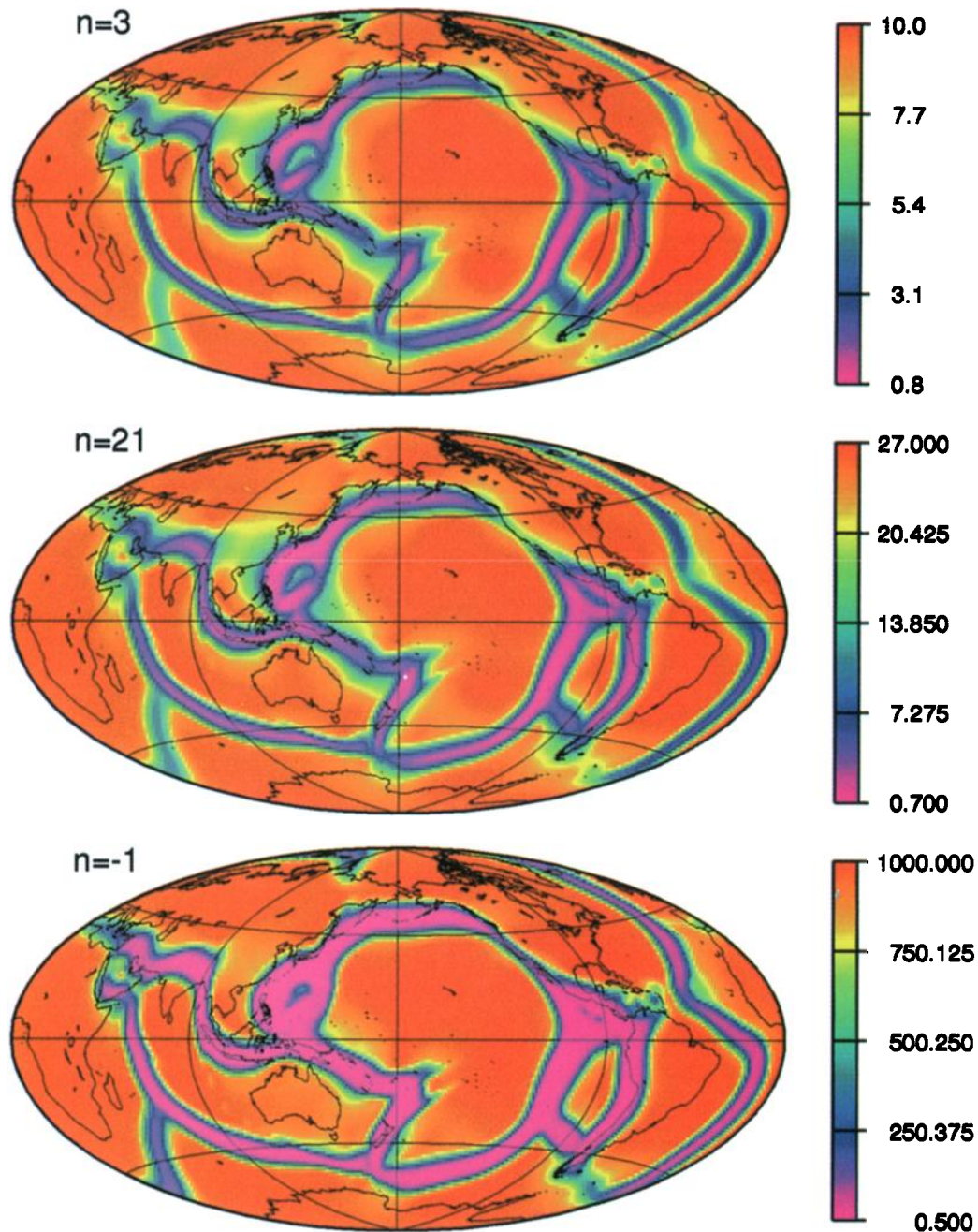


Plate 3. Viscosity fields for the same non-Newtonian solutions of Plates 2. Color scale is unstretched.

feature of platelike motion. In particular, the high viscosity contrast power law cases (with $\gamma = 5 \times 10^{-7}$; see Figure 6) display particularly little plateness, especially with regard to their viscosity fields. In contrast, the WG and low viscosity contrast ($\gamma = 10^{-3}$) power law rheologies generate quite high plateness. The $\gamma = 5 \times 10^{-7}$ cases, however, yield values of KE_T/KE_P and Ω (particularly at smaller n) which are comparable to those of the WG case and significantly more platelike than those of the $\gamma = 10^{-3}$ power law cases. Thus, although “plateness” and toroidal motion with significant magnitude are desirable goals for a model of plate generation,

they may have little to do with one another and probably must be attained independently. Rather than being a further obfuscation of the plate-mantle coupling problem, this point in fact suggests that “plateness” and the magnitude of toroidal motion are two independent constraints which make the problem of finding a plate-mantle rheology more well-determined.

Self-Lubrication Versus Power Law Rheologies

Bercovici [1993] suggested that power law rheologies are not sufficient to allow plate tectonics to arise from mantle flow and that self-lubricating rheologies, such as

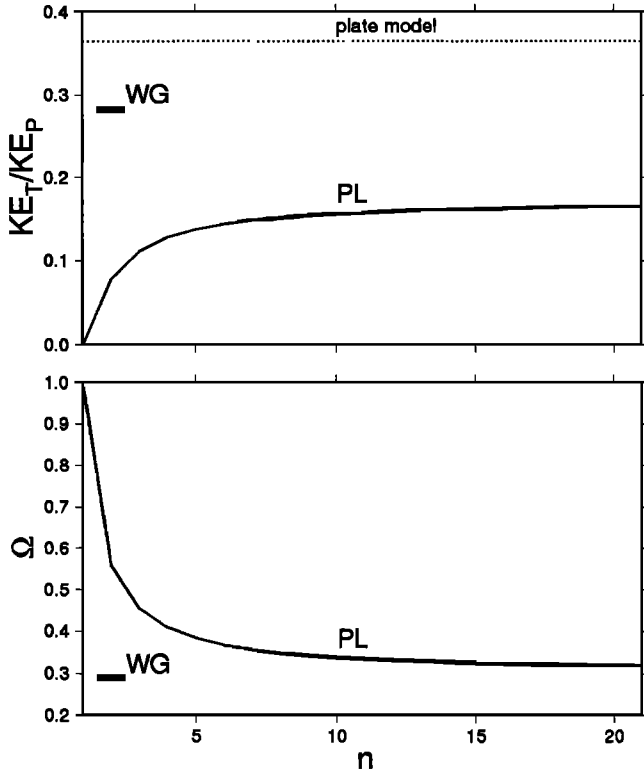


Figure 8. Toroidal-poloidal kinetic energy ratio $\overline{KE_T}/\overline{KE_P}$ and vorticity deviation Ω versus power-law index n for power-law cases (using the source-sink field of Plate 1). The values of $\overline{KE_T}/\overline{KE_P}$ for the WG case and $\overline{KE_T}/\overline{KE_P}$ for the plate model are shown for comparison. As with Plates 2 and 3, $\gamma = 10^{-3}$ for all flow solutions shown. See Plate 2 for discussion of convergence error.

the WG rheology, are necessary to adequately generate plates. In this paper we have shown that this suggestion applies in a spherical coordinate system and to realistic plate geometries. None of the rheologies examined in fact reproduces the original plate models perfectly. Yet, the WG stick-slip rheology generates the best combination of platelike qualities, i.e., relatively large values of the kinetic energy partitioning ratio $\overline{KE_T}/\overline{KE_P}$, small values of vorticity deviation Ω and very platelike flow and viscosity fields. Power law rheologies with high viscosity contrasts yield reasonably platelike values of $\overline{KE_T}/\overline{KE_P}$ and Ω (at least comparable to those for the WG rheology), but the shape of their flow and viscosity fields are not platelike. For power law rheologies with low viscosity contrast the opposite is true (more or less). However, even the WG rheology requires sufficiently large viscosity contrasts (i.e., small γ) to yield platelike flows. More specifically, the self-lubricating mechanism is most effective when strain rates significantly exceed the “cutoff” strain rate of $\sqrt{-n\gamma}$ and are thus in the self-lubricating regime (see Figure 1); for strain rates beneath this value the fluid merely acts as an extremely viscous medium.

Future Avenues

The self-lubricating rheology employed in this paper is of course an ad hoc formulation designed to capture the basic nature of the stress-strain rate relation with minimum complication. Actual self-lubrication mechanisms involve more complicated physics such as the feedback effect of shear heating in fluid with temperature-dependent viscosity [Schubert and Turcotte, 1972; Yuen

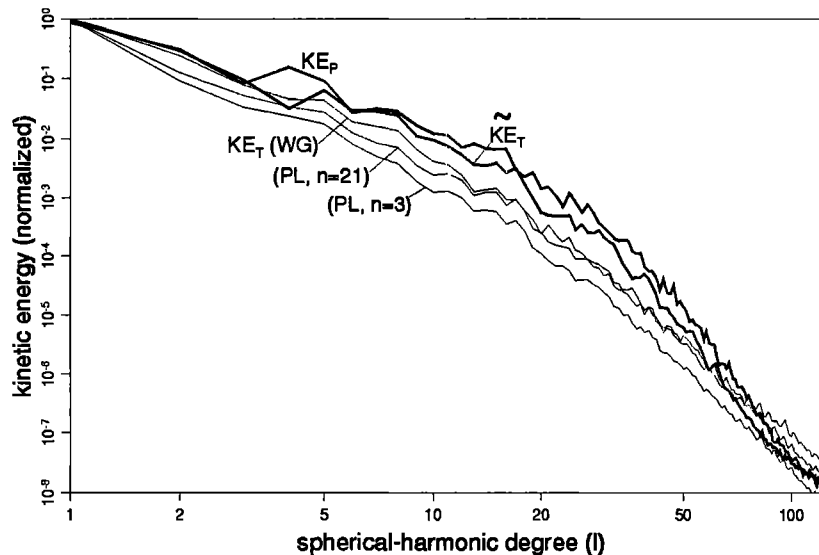


Figure 9. Spherical harmonic power spectra for toroidal and poloidal kinetic energies for the plate model (thick curves) and toroidal energy for the non-Newtonian solutions. All curves are normalized by the maximum power. The $l = 1$ toroidal energy is added to the non-Newtonian curves to prevent logarithmic singularities. The $\overline{KE_P}$ curve shows $l(l+1)|\Phi_l^m|^2$; the $\overline{KE_T}$ curve shows $|\tilde{\omega}_l^m|^2/[l(l+1)]$; the $\overline{KE_T}$ curves all show $l(l+1)|\Psi_l^m|^2$.

and Schubert, 1979]; indeed the WG rheology can be derived from a simple model of this effect [Whitehead and Gans, 1974]. Another example may involve the lubricating effect of water as it is drawn (in various manners) into plate margins [e.g., Lenardic and Kaula, 1994]; this of course has been postulated to account for Earth's unique form of surface tectonics [Tozer, 1985; Kaula, 1990]. A natural avenue for work on plate generation is therefore to incorporate more physically based self-lubricating mechanisms into a nonlinear rheology.

The source-sink formulation employed in this study and by Bercovici [1993] yields perhaps the simplest possible model of toroidal flow generation (since the poloidal flow is entirely specified). The geometry of the sources and sinks, however, tends to overconstrain the plate formation problem; i.e., the plate geometries are at least 50% prescribed by the source-sink field; thus the formation of plates is not completely self-determined by the fluid dynamics. A more self-consistent formulation (short of accounting for underlying mantle flow as by Ribe [1992] and Weinstein and Olson [1992]) would be to specify only the sink field and allow the sources to be generated from the poloidal equation of motion (in particular the radial component of the momentum equation or $\underline{r} \cdot \nabla \times \nabla \times (5)$). This is essentially analogous to driving lithospheric motion only with subducting slabs, presumed to be the main source of gravitational potential energy release in the mantle.

If tractable, these rheological and kinematic extensions of the model (to essentially incorporate more self-consistent physics) will be the next step to finding how plate tectonics arises from mantle dynamics as a self-determined, self-organizing structure.

Acknowledgments. The author thanks Stuart Weinstein, Pål Wessel, Peter Olson, and Brian Taylor for useful discussions and C.W. Gable, R.J. O'Connell, and F.D. Stacey for helpful reviews. This work was supported by NASA grant NAGW-3015.

References

- Bercovici, D., A simple model of plate generation from mantle flow, *Geophys. J. Int.*, **114**, 635-650, 1993.
- Bercovici, D. and P. Wessel, A continuous kinematic model of plate tectonic motions, *Geophys. J. Int.*, **119**, 611-626, 1994.
- Bird, R.B., R.C. Armstrong, and O. Hassager, *Dynamics of Polymeric Liquids*, vol. 1, Wiley-Interscience, New York, 1987.
- Chandrasekhar, S., *Hydrodynamic and Hydromagnetic Stability*, Oxford University Press, New York, 1961.
- Christensen, U., and H. Harder, Three-dimensional convection with variable viscosity, *Geophys. J. Int.*, **104**, 213-226, 1991.
- DeMets, C., R.G. Gordon, D.F. Argus, and S. Stein, Current plate motions, *Geophys. J. Int.*, **101**, 425-478, 1990.
- Forte, A.M. and W.R. Peltier, Plate tectonics and aspherical earth structure: The importance of poloidal-toroidal coupling, *J. Geophys. Res.*, **92**, 3645-3679, 1987.
- Gable, C.W., R.J. O'Connell, and B.J. Travis, Convection in three dimensions with surface plates: Generation of toroidal flow, *J. Geophys. Res.*, **96**, 8391-8405, 1991.
- Glatzmaier, G.A., Numerical simulations of stellar convective dynamos. I, The model and method, *J. Comput. Phys.*, **55**, 461-484, 1984.
- Gurnis, M., and B.H. Hager, Controls of the structure of subducted slabs, *Nature*, **335**, 317-321, 1988.
- Hager, B.H., and R.J. O'Connell, Subduction zone dip angles and flow driven by plate motion, *Tectonophysics*, **50**, 111-133, 1978.
- Hager, B.H., and R.J. O'Connell, Kinematic models of large-scale flow in the Earth's mantle, *J. Geophys. Res.*, **84**, 1031-1048, 1979.
- Hager, B.H., and R.J. O'Connell, A simple global model of plate dynamics and mantle convection, *J. Geophys. Res.*, **86**, 4843-4867, 1981.
- Kaula, W.M., Material properties for mantle convection consistent with observed surface fields, *J. Geophys. Res.*, **85**, 7031-7044, 1980.
- Kaula, W.M., Venus: A contrast in evolution to Earth, *Science*, **247**, 1191-1196, 1990.
- Kaula, W.M., and D.R. Williams, Transformations of velocity fields on a spherical surface, in *Geodesy in Transition*, edited by K.P. Schwarz and G. Lachapelle, pp.177-183, University of Calgary, Alberta, 1983.
- King, S.D., and B.H. Hager, The relationship between plate velocity and trench viscosity in Newtonian and power-law subduction calculations, *Geophys. Res. Lett.*, **17**, 2409-2412, 1990.
- Lachenbruch, A.H., Dynamics of a passive spreading center, *J. Geophys. Res.*, **81**, 1883-1902, 1976.
- Lenardic, A., and W.M. Kaula, Self-lubricated mantle convection: Two-dimensional models, *Geophys. Res. Lett.*, **21**, 1707-1710, 1994.
- Lithgow-Bertelloni, C., M.A. Richards, Y. Ricard, R.J. O'Connell, and D.C. Engebretson, Toroidal-poloidal partitioning of plate motions since 120 Ma, *Geophys. Res. Lett.*, **20**, 375-378, 1993.
- Minster, J.B., and T.H. Jordan, Present-day plate motions, *J. Geophys. Res.*, **83**, 5331-5354, 1978.
- Minster, J.B., T.H. Jordan, P. Molnar, and E. Haines, Numerical modelling of instantaneous plate tectonics, *Geophys. J. R. Astron. Soc.*, **36**, 541-576, 1974.
- Morgan, W.J., Rises, trenches, great faults, and crustal blocks, *J. Geophys. Res.*, **73**, 1959-1982, 1968.
- O'Connell, R.J., C.W. Gable, and B.H. Hager, Toroidal-poloidal partitioning of lithospheric plate motion, in *Glacial Isostasy, Sea Level and Mantle Rheology*, edited by R. Sabadini et al., pp. 535-551, Kluwer Academic, Norwell, Mass., 1991.
- Olson, P., and D. Bercovici, On the equipartitioning of kinetic energy in plate tectonics, *Geophys. Res. Lett.*, **18**, 1751-1754, 1991.
- Ranalli, G., *Rheology of the Earth*, Allen and Unwin Publishers, Winchester, Mass., 1987.
- Ribe, N.M., The dynamics of thin shells with variable viscosity and the origin of toroidal flow in the mantle, *Geophys. J. Int.*, **110**, 537-552, 1992.
- Ricard, Y., C. Doglioni, and R. Sabadini, Differential rotation between lithosphere and mantle: A consequence of lateral mantle viscosity variations, *J. Geophys. Res.*, **96**, 8407-8415, 1991.
- Schubert, G., and D.L. Turcotte, One-dimensional model of shallow mantle convection, *J. Geophys. Res.*, **77**, 945-951, 1972.
- Tozer, D.C., Heat transfer and planetary evolution, *Geophys. Surv.*, **7**, 213-246, 1985.
- Washington, W.M., and C.L. Parkinson, *An Introduction to Three-Dimensional Climate Modeling*, Appendix B, Oxford University Press, New York, 1986.
- Weertman, J., and J.R. Weertman, High temperature creep

- of rock and mantle viscosity, *Annu. Rev. Earth Planet. Sci.*, *3*, 293–315, 1975.
- Weinstein, S., and P. Olson, Thermal convection with non-Newtonian plates, *Geophys. J. Int.*, *111*, 515–530, 1992.
- Whitehead, J.A., and R.F. Gans, A new, theoretically tractable earthquake model, *Geophys. J. R. Astron. Soc.*, *39*, 11–28, 1974.
- Yuen, D.A., and G. Schubert, The role of shear heating in the dynamics of large ice masses, *J. Glaciol.*, *24*, 195–212, 1979.
-
- D. Bercovici, Department of Geology and Geophysics, School of Ocean and Earth Science and Technology, University of Hawaii, 2525 Correa Road, Honolulu, HI 96822. (e-mail: dberco@soest.hawaii.edu)

(Received April 11, 1994; revised September 21, 1994; accepted September 29, 1994.)